Nanoscale

Dynamic Article Links

Cite this: *Nanoscale*, 2011, **3**, 4182

www.rsc.org/nanoscale

PAPER

Probing the local structure of dilute Cu dopants in fluorescent ZnS nanocrystals using EXAFS

Brad Car,[a] Scott Medling,*[a] Carley Corrado,[b] Frank Bridges[a] and Jin Z. Zhang[b]

Received 31st May 2011, Accepted 17th July 2011
DOI: 10.1039/c1nr10556f

A local structure study of ZnS nanocrystals, doped with very low concentrations of Cu, was carried out using the EXAFS technique to better understand how Cu substitutes into the host lattice and forms Cu luminescence centers. We show that a large fraction of the Cu have three nearest neighbor S atoms and the Cu–S bond is significantly shortened compared to Zn–S, by ~0.08 Å. In addition, the second neighbor Cu–Cu peak is extremely small. We propose that Cu occupies an interior site next to a S^{2-} vacancy, with the Cu displaced towards the remaining S^{2-} and away from the vacancy; such a displacement immediately explains the lack of a significant Cu–Cu peak in the data. There is no evidence for interstitial Cu sites (Cu_i), indicating that no more than 2% of the Cu are Cu_i. This study provides new insights into the local structure of the Cu dopant in ZnS without the presence of CuS nanoprecipitates that are present at higher Cu doping levels.

1 Background

ZnS phosphors, co-doped with Cu and other co-activators (Cl, Br, Al), have been studied extensively[1,2] since they were found to exhibit AC electroluminescence (EL)[3] at relatively low applied AC electric fields. In the last few years, these materials have received renewed attention for both bulk and nano materials.[4–13] Both EL and photoluminescence (PL) arise from electron-hole recombinations of charges excited (either electrically or optically) into trap states; the dominant emission in both cases is a strong blue band which is observed in both bulk and nanocrystal (NC) ZnS:Cu.[1,9,13] Cl^-, Br^-, and Al^{+3} form the electron trap sites while dilute Cu centers form the hole trap sites. Cu is only slightly soluble in ZnS (up to roughly 0.04% Cu in ZnS) and, when the Cu concentration is above the solubility threshold, conducting CuS precipitates form as the crystal cools.[2,14] These conducting needle-like precipitates enhance the local electric fields about the precipitate tips when the electric field is reversed in AC operation and lead to the low voltage AC EL.[14]

However, the actual transitions that lead to the blue lines are still under debate. As we noted earlier for bulk materials,[13] there are three blue lines at similar energies: a blue line in Cl^-(or Br^-) doped (and some undoped) materials with the hole trap associated with a Zn vacancy complex[15] (V_{Zn}, Cl_s^-, 3 S^{2-}), a blue line for Cu doped (no Cl^-), and a similar line with both Cl and Cu doping associated with a Cu complex hole trap. In contrast, recent studies have suggested that the blue PL emission of undoped ZnS NCs arises from V_S donor traps in the host lattice, but the hole trap is not defined.[4,16–21] Indirect evidence of V_S has been shown by energy-dispersive X-ray spectroscopy (EDS) showing an excess of Zn over S in ZnS NCs,[18,21] as well as inductively-coupled plasma (ICP) yielding the same result.[4] Because of the large surface area in NCs, the excess of Zn over S could also arise because of the excess Zn on the surface of the NCs, rather than V_S. This possibility is not unlikely since the capping ligands are often negatively charged and generally bind to Zn. Without an excess of Zn, the surface is not as well protected, leading to quenched emission. For this reason, the excess of Zn over S cannot unequivocally be assigned to S vacancies. Similarly, the blue PL emission in Cu-doped ZnS NCs has been attributed to electronic transition from V_S donor trap states below the conduction band to deep trap states above the valence band created by Cu.[19–21] Most of both the old and recent literature agree that the V_S donor state is about 0.6–0.8 eV below the conduction band. Then to have the blue line emission at ~ 2.8 eV, the deep trap state must be close to the valence band, at least 3.5 eV below the conduction band. While this is inconsistent with the ~ 1 eV splitting between the e_g and t_{2g} energy levels for Cu centers in bulk ZnS with t_{2g} about 1.3 eV above the valence band,[22,23] it might be partially due to quantum confinement increasing the bandgap of the ZnS, plus a shift of the Cu levels in ZnS NCs.

Thus, a long-standing question about ZnS:Cu phosphors still remains unanswered: what is the local structure of the luminescent emission centers that are associated with the low concentration Cu sites? Several models have been proposed but local structure details are limited. Because of the low solubility of Cu in ZnS, definitive studies need to be done at very low Cu concentrations where precipitates have not formed. In addition, the evidence for V_S trap states is also indirect, and there may be isolated V_S as well as complex centers, with V_S associated with

[a]*Physics Department, UC Santa Cruz. E-mail: smedling@ucsc.edu*
[b]*Chemistry Department, UC Santa Cruz*

some other defect. Here, for the first time, we address the local structure about Cu using EXAFS studies of a number of low concentration NC samples in conjunction with spectroscopic studies. The analysis suggests that a S vacancy exists on one of the nearest neighbor sites about the Cu dopants.

Early work established, with a few ppm sensitivity, that all the Cu atoms in bulk ZnS:Cu are diamagnetic and hence Cu (including the Cu atoms that form the CuS precipitates) is in the +1 valence state when the material has not been excited—either optically or electrically.[24,25] Our NC ZnS:Cu,Cl samples also show no Electron Spin Resonance (ESR) signal at liquid helium temperatures when unexcited, while a signal emerges when excited with UV light as noted earlier for bulk material by Holton.[25] For the isolated Cu atoms in the ZnS host (*i.e.*, not in CuS precipitates), the +1 valence state requires other nearby defects for charge compensation. Cu^+ has a d^{10} configuration and is not paramagnetic, but when it is excited by trapping a hole, it temporarily has a d^9 configuration and is optically active and paramagnetic. In PL, the blue line generally dominates but a green line is also observed[22] while in EL three major, closely-spaced, blue/green lines are observed plus a weak (2–3%) narrow line.[13] Some have also reported a red line in bulk ZnS:Cu when there are significant S vacancies present.[26] Since a similar red line has not been reported for NCs, we do not consider it further. An important additional property of the center(s) responsible for the blue PL line dominant in our samples is that they likely have local C_{3v} symmetry based on Raman studies of single crystals,[27] and hence these Cu atoms are not in a site with the simple tetrahedral symmetry of the zincblende lattice.

A number of charge compensated Cu-complex models have been suggested for these low concentration emission centers.[1,2,4,22,23,27–30] The main models discussed in the literature are: two substitutional Cu^+ atoms on Zn sites, Cu^+_{Zn}, adjacent to a S^{2-} vacancy, substitutional Cu^+_{Zn} plus substitutional Cl^- on a neighboring S^{2-} site, $Cl_S{}^-$, and a Cu pair formed of substitutional Cu^+_{Zn} plus a nearby interstitial Cu atom, Cu_i^+ [4,27,29] Cu^+_{Zn} adjacent to either a S^{2-} vacancy or a Cl^-_S defect will have C_{3v} symmetry while the most likely Cu_i site (site I_1 with four S nearest neighbors) does not; a second interstitial site (site I_2 with four Zn/Cu nearest neighbors) would have C_{3v} symmetry if one of the four nearest neighbors was Cu. These sites are shown in Fig. 16 of the paper by Stanley *et al.*[13] Additional complexity arises if the S vacancy, Cl^-_S, or interstitial Cu_i are on more distant sites.

A more important consideration is that the Cu 3d-states split into e_g (lower) and t_{2g} (upper) multiplets in the tetrahedral crystal field of the zincblende lattice. Under C_{3y} reduced symmetry, the t_{2g} multiplet splits further into e'_g and a_{1g}. Consequently, there may be three possible hole trap states for an activated Cu site that could lead to three distinct optical emission lines. Such a variety of possibilities may explain why in ESR experiments, $T \leq 4$ K, as many as seven distinct (metastable) ESR signals associated with Cu can be produced by UV activation.[25] Because ESR is an extremely sensitive probe and can see defects at the ppm level, some of the centers observed may be extremely dilute. However, because there are only 3 dominant optical emissions in our earlier studies,[13] we focus on these dominant centers.

In this work, we can directly address three questions about the charge compensation from near neighbors: 1) is there a significant fraction of Cu^+_{Zn} defects with a charge compensating nearest neighbor S vacancy, leaving only three S neighbors, 2) do adjacent Cl^-_S defects provide most of the charge compensation, or 3) do a significant fraction of interstitial sites, Cu_i, exist? We have partially addressed the last question in studies of bulk ZnS:Cu particles[13] and some higher concentration Cu-doped ZnS NCs;[9] however because these Cu-doped NCs had concentrations well above the Cu solubility limit, there may have been CuS clusters, limiting our ability to exclude interstitial sites to $\sim$ 10%. To provide a more definitive upper limit on the fraction of Cu in interstitial sites, we use ZnS NCs with very low Cu concentrations, $\sim$ 0.02% and 0.04% Cu. For these concentrations, and NC diameters below 6 nm, the average number of Cu atoms/particle is < 1; so little or no clustering should be present.

2 Experimental details

Five ZnS:Cu,Cl NC samples were synthesized by an aqueous precipitation method, as in the paper by Corrado *et al.*[9] Three of the samples have $\sim$0.02% Cu (samples A1, A2, and A3) while the other two contain $\sim$0.04% Cu (samples B1 and B2). Briefly, Zn $(NO_3)_2 \cdot 6H_2O$, $CuCl_2 \cdot 2H_2O$, and mercaptopropionic acid (MPA) were combined in milli-Q water. The pH was adjusted to 11 using NaOH. Next, the solution was degassed after which $Na_2S \cdot 9H_2O$ was injected quickly. It was stirred for 15 min, then exposed to air. The reaction mix was then refluxed 1 h while excess Zn ($Zn(NO_3)_2$ $6H_2O$) was added. The NCs were precipitated by addition of ethanol, centrifuged, washed several times with ethanol, and finally lyophilized.

The UV-vis absorption spectra were taken on a HP 8452A diode array spectrophotometer at room temperature. The PL spectra were measured on a Perkin-Elmer LS50B luminescence spectrometer at room temperature. The samples that were analyzed with spectrophotometry were prepared by dispersing the NCs in milli-Q water, basified to pH $\sim$ 11 with NaOH, to yield a clear solution.

The EXAFS samples were prepared by dissolving the cleaned NC powder in a few drops of milli-Q water. The concentrated solution was then dropped onto filter paper with the dimensions 3 mm by 13 mm. The filter paper, saturated in NCs, was then sandwiched between two glass slides and warmed on a hotplate to evaporate the water without the edges curling up. Each dried filter paper plus NC sample was then encased in Scotch tape to contain the NCs, several layers of which were stacked together such that the step height at the Zn K-edge absorption was in the range 0.3–1.

EXAFS and XANES data for the ZnS:Cu,Cl NCs (3–6 nm in diameter) were collected at 10 K at the Stanford Synchrotron Radiation Lightsource (SSRL) on beamline 10–2 using a Si [111] double monochromator detuned by 50% to reduce harmonics. A slit height of 0.6 mm provided an energy resolution of $\sim$ 1.5 eV. The Zn K-edge data were collected in transmission mode; the Cu K-edge data were collected in fluorescence mode using a 13 element Ge detector with the samples at 45° to the incident beam. For both types of data sets, a pre-edge subtraction was applied using standard procedures (RSXAP).[31]

Because of the very low Cu concentration, the weak Zn Raman line from ZnS becomes an important background contribution in a Cu scan; this peak is at a fixed energy below the incident X-ray energy[32] and grows in amplitude as the incident X-ray energy

approaches the Zn K-edge. During a Cu scan, the Zn Raman peak passes through the fluorescence window set up for Cu. In addition, very close to the Zn K-edge at the top of the Cu scan, the tail of the Zn fluorescence peak also produces a background within the Cu fluorescence window. These background contributions were subtracted by conducting a Cu scan on Zn foil, fitting to a 6th order polynomial, and then weighting and subtracting this background function from the low concentration Cu scans.[33]

These corrected data were then re-reduced using standard procedures (RSXAP)[31] to obtain k-space data, $k\chi(k)$, and then averaged over 5 scans to improve the signal-to-noise for these very dilute samples. Examples of the k-space data are shown in Fig. 1 for three samples; two with 0.02% Cu (A1 and A2) and one with 0.04% Cu (B2). Scans for the other two samples were similar. Although the scans become noisy at high k, they have nearly identical structure up to $k \sim 11$ Å^{-1} and we use the data up to $k = 10.5$ Å^{-1} to Fast Fourier Transform (FFT) the k-space data to r-space using an FFT window of 3.5–10.5 Å^{-1} with a Gaussian rounding of 0.3 Å^{-1}.

3 Optical properties

The PL emission spectra of ZnS:Cu (0.04%) compared to the PL emission of ZnS:Cu (1%) are shown in Fig. 2, along with the UV-vis spectrum of the 0.04% sample. The UV-Vis absorption spectrum shows an absorption onset around 330 nm and features a small peak around 310 nm and an apparent strong peak around 230 nm. The peak near 230 nm is likely an artifact due to the unreliable instrument response in that region. The excitonic peak at 310 nm is due to bandgap excitation of the host and is indicative of the small size of the NCs. The UV-Vis spectra of undoped and Cu doped ZnS NCs are indistinguishable, indicating that Cu-doping has no or little effect on the electronic absorption spectrum of ZnS. This is not surprising due to the low doping level.

The PL emission spectrum of the ZnS:Cu (0.04%) shows a broad emission band around 445 nm with a FWHM of 90 nm. The emission from this sample is indistinguishable from that of the undoped ZnS NCs because it contains such a low concentration of Cu. The ZnS:Cu (1%) sample exhibits a red-shifted emission band around 465 nm, which confirms successful Cu doping, as our previous work shows the dependence of the PL emission peak position on the concentration of Cu.[9]

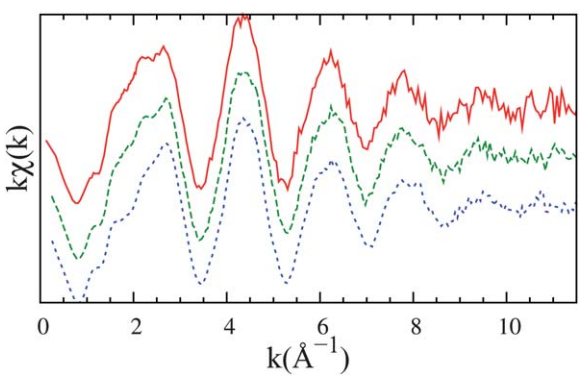

Fig. 1 Averaged k-space data for three ZnS:Cu samples, top to bottom: A1–Cu 0.02% (solid red), A2–Cu 0.02% (dashed green), and B2–Cu 0.04% (dotted blue).

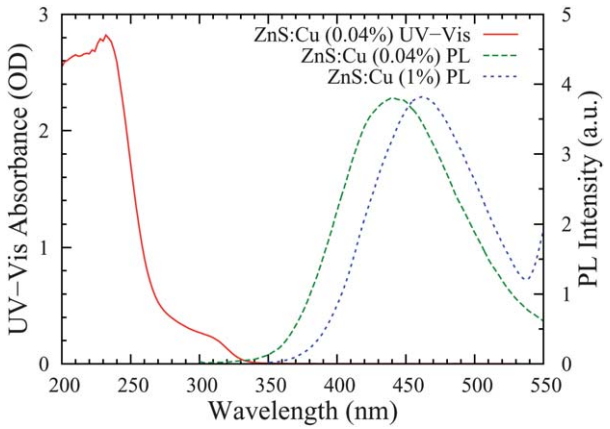

Fig. 2 UV-vis and PL spectra of ZnS:Cu (0.04%) (red and green lines) and ZnS:Cu (1%) (blue line).

4 Cu K-edge EXAFS data

Examples of the averaged r-space Cu K-edge data for two different 0.02% Cu samples (A1 and A2), and a 0.04% Cu sample (B2) [same samples as in Fig. 1], are shown in Fig. 3 and compared with the corresponding Zn K-edge data, and a simulation for Zn on the surface, to be discussed later. Note that the EXAFS r-space position is slightly shorter than the actual position; this difference arises from a well known phase shift[34] and is included in the fits. All three Cu traces are nearly identical (as are A3 and B1, not shown), indicating the same local structure in each sample. The first peak near 1.8 Å (actual distance ~2.3 Å) corresponds to the nearest neighbor S atoms in cubic ZnS; the next peak for this structure, assuming substitutional Cu^{+}_{Zn}, corresponds to twelve Zn neighbors and should occur near 3.6 Å (actual distance 3.8 Å). However, there is no obvious peak between 3 and 4 Å for the Cu K-edge data in Fig. 3 a-c. It is very surprising that this peak is so weak since it is present in the Zn K-edge data for the NCs (see Fig. 3d), and even a Cu site close to the surface would have 4–6 Zn second neighbors and lead to a visible, although reduced, second neighbor peak (see Fig. 3e).

If there is also some interstitial Cu, there are two possibilities as described above. Site I_1 would again have four S nearest neighbors and the first Cu–S peak in the EXAFS plot would be near 1.8 Å. However, the next peak for this interstitial Cu site would occur near 2.4 Å in the EXAFS plot (actual distance 2.7 Å) and correspond to six Zn neighbors. Since the amplitude near 2.4 Å is very low, there cannot be much interstitial Cu of this type. The second interstitial site, I_2, has four Zn/Cu neighbors at ~ 2.34 Å, the same distance as for Zn–S in ZnS. We address both possibilities below.

5 Cu K-edge XANES data

The analysis of the EXAFS data (discussed below) suggests that the Cu is in a distorted site and likely near a S vacancy. Since the edge is often sensitive to local distortions of the environment about the probed atom, we also examined the Cu XANES (X-ray

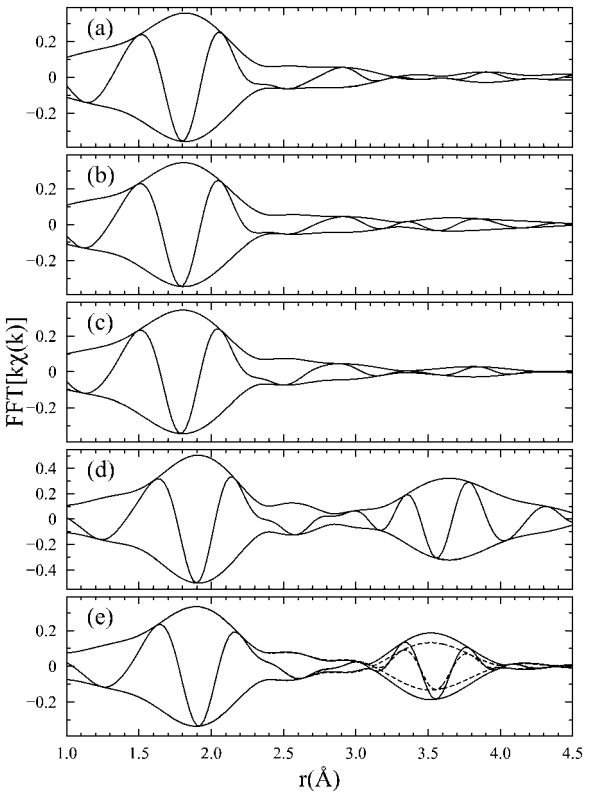

Fig. 3 R-space data for three ZnS:Cu samples: (a) A1, 0.02% Cu, (b) A2, 0.02% Cu, (c) B2, 0.04% Cu. (d) The corresponding FFT for Zn K-edge data over the same FFT range, and (e) a simulation for Zn on the particle surface, with 3 S neighbors and either 4 (dashed) or 6 (solid) Zn neighbors. A significant global broadening, $\sigma^2 \sim 0.006$ Å^2, was included for (e). Here and in later plots, the fast oscillation is the real part of the FFT, R, while the envelope is $\pm \sqrt{R^2 + I^2}$, where I is the imaginary part of the FFT.

absorption near edge structure) for these and similar samples at higher Cu concentrations. In Fig. 4 we plot the edges for several samples and compare them to two reference samples, Cu metal and a Cu_2S bulk powder.

The XANES for the four ZnS:Cu samples are very similar and have little structure—a small amplitude variation at the top of the edge (8990–9010 eV) and tiny variations in weak structure along the edge, such as the feature at the half height point on the edge. In addition, the edge for bulk Cu_2S is very similar to ZnS:Cu, but has even less structure. Note that the environment about Cu in the complex Cu_2S structure is quite different from that for Cu on the Zn site in ZnS and that the average edge passes through the middle of the Cu foil edge.

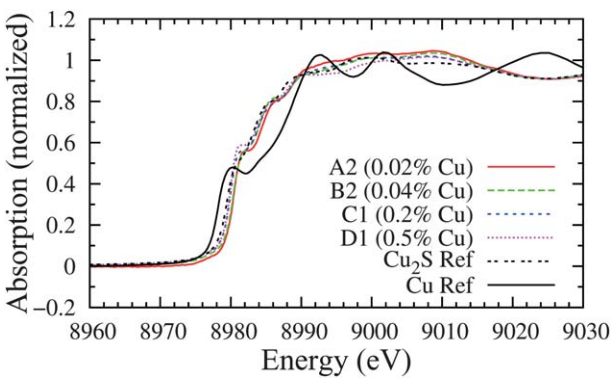

Fig. 4 Plots of the Cu XANES for ZnS:Cu for concentrations 0.02, 0.04, 0.2, 0.5% and two reference materials Cu_2S and Cu metal. The scans were normalized at higher energies.

We also used FEFF8.20[35] to calculate the XANES for Cu on an undistorted Zn site with four S neighbors, for Cu on an undistorted Zn site with three S neighbors and a vacancy, and for Cu next to a vacancy but displaced away from the vacancy. These simulations do not look similar to the measured edges; they show significant structure that changes as the environment varies. We had similar difficulties in simulating the edge for CuS; Rehr[36] suggested that the potentials for sulfides, needed to simulate the Cu K-edge XANES, are not yet good enough for a quantitative comparison. Despite this limitation of the XANES modeling to elucidate the local distortions, the experimental XANES data are similar over a wide Cu concentration range and the positions are clearly consistent with a Cu 1+ oxidation state.

6 EXAFS data analysis and discussion

To quantify whether or not a significant Cu–Zn peak exists near 2.4 Å (for interstitial Cu_i site I_1) requires a careful comparison between two fits: one with an interstitial peak and one without. We initially fit the r-space data using theoretical standard EXAFS functions calculated using FEFF8.20.[35] Here we used the known ZnS structure (F-43m, a = 5.412) but replaced the central Zn atom with Cu. The standard for the short Cu–Zn interstitial peak ($\sim$ 2.7 Å; six Zn neighbors) was also calculated using FEFF by placing the central Cu atom at the interstitial positions in ZnS.

Because the possible interstitial Cu–Zn peak at 2.7 Å must be small and would occur on the high side of the Cu–S peak, a further complication exists; for many other systems, we have found a systematic deviation on the high-r side of the first r-space peak between EXAFS functions calculated using FEFF and the corresponding experimental standards.[37–39] This small deviation can look like a weak peak. Thus in addition to using the Cu–S function calculated from FEFF for r = 2.343 Å, we also generated an experimental Cu–S standard from the Zn–S peak in Zn K-edge data for ZnS NCs following the procedures described in detail by Li *et al.*[38] We compare these two Cu–S functions in Fig. 5; here, we have fit the experimental standard using the FEFF function by varying r, σ (width of the pair distribution function), the amplitude, and a small E_o shift. For this experimental Cu–S function, the S_o^2 parameter is 0.98; other parameters are given in Fig. 5. This comparison shows that the difference between the theoretical and experimental functions on the high-r side of the Cu–S peak is quite small (smaller than observed in many other systems).

An even more important benefit of using an experimental standard is that it also provides a more accurate means of estimating the number of S neighbors about Cu, because the standard described above was made from a NC sample (same sample geometry), and has exactly four S neighbors. In particular, when using the experimental standard there is no amplitude correction factor (*i.e.* $S_o^2 = 1$) as is generally needed when using FEFF

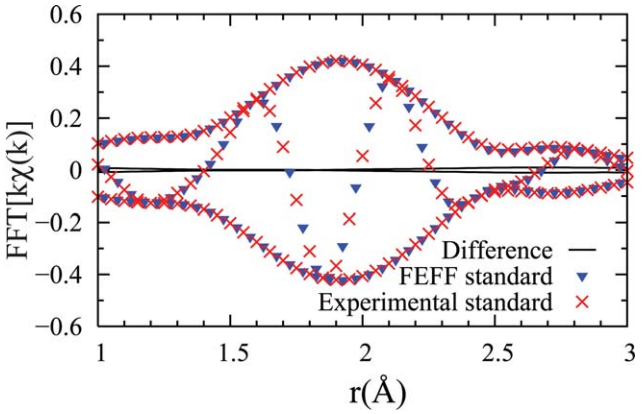

Fig. 5 Experimental and theoretical Cu–S standards in r-space. Note the nearly identical shapes. We fit the experimental function using the FEFF standard over the r-range 1.2–2.5 Å; the fit parameters are r = 2.345 Å, σ = 0.064 Å, E_o shift = −9.4 eV and $S_o^2 = 0.98$.

standards; then the amplitude = $N \cdot S_o^2$ where N is the coordination number, and these two factors cannot be separated.

We first carried out 1-peak fits in r-space using FEFF and experimental Cu–S functions over a short r-space range (1.4–2.2 Å). For all samples, the results for the 1-peak fits are very similar, as was expected from the similar r-space scans in Fig. 3. The main difference between using FEFF and experimental Cu–S functions is a difference in σ, since the experimental function already includes some thermal motion disorder ($\sigma^2 = 0.0041$ Å^2) while the FEFF standard does not. We have from 4–7 scans for each of the five samples; 25 scans in total. Each scan is fit separately and then the average of the amplitudes and σ^2 (or $\Delta\sigma^2$ for the experimental standard) were determined for each sample. The RMS variation in the number of neighbors is <0.2, as determined from variations between the 5 scans for each sample.

These 1-peak fits done with an experimental Cu–S function show that the number of S neighbors varies between 3.0 and 3.3 for all samples (see Table 1). Thus, a significant fraction of Cu atoms must have a nearest neighbor S vacancy, in some cases perhaps as a result of Cu being near the surface. Since the NCs were synthesized with a very slight deficiency of S and the surface is expected to be rich in Zn atoms over S, this must be considered. However, because the Zn K-edge data show no evidence for S vacancies about Zn, and since no red emission line (associated with excess S vacancies[26]) is observed, the overall concentration of S vacancies must be small. The change in the PL data with Cu concentration[9] shows that Cu is incorporated into the ZnS NCs but provides no information about the local environment; however, the EXAFS data are primarily consistent with defect models for which the Cu^+_{Zn} defects are compensated by nearest neighbor S vacancies.

Table 1 Number of S nearest neighbors about Cu. Fit using the experimental Cu–S function with an r-range of 1.4–2.2 Å and FFT range of 3.5–10.5 Å^{-1}. RMS variation in the number of neighbors is < 0.2. Decreasing the FFT range to 4–9 Å^{-1} slightly increases the number of neighbors by 0.1–0.2

# of S neighbors	A1	A2	A3	B1	B2
1-peak fit	3.2	3.0	3.0	3.1	3.0
multipeak fit	3.3	3.1	3.0	3.1	3.1

Because Cl is a neighbor to S in the periodic table, the S and Cl backscattering functions are too similar to be able to differentiate between S and Cl neighbors and the fact that the Shannon ionic radii are nearly identical means there is no expected significant lattice distortion; thus, a few of the ∼ 3–3.3 nearest neighbors might actually be Cl. However, Cl^- on a S^{2-} site will charge compensate Cu^+_{Zn} defects, so we do not expect both a S vacancy and Cl^- as nearest neighbors for a given Cu site. The large number of nearest neighbor S vacancies about Cu, inferred from the decreased coordination number (∼ 3 instead of 4), suggests that the number of nearest neighbor Cl^- is likely small.

As to the question of whether the Cu dopants are mostly in the surface layer *versus* on interior sites, a second result from the 1-peak fits is that the Cu–S distances are shorter than the Zn–S distance of the host lattice; 2.26–2.27 Å for the 0.02% and 0.04% Cu samples, compared to 2.34 Å for Zn–S. Since, as discussed above, a large fraction of Cu sites have a missing S neighbor, we consider two cases: Cu at an interior site with a neighboring S vacancy, and Cu at the surface. For the interior site, the short Cu–S distance may arise from a [111] displacement of Cu—attracted towards the three remaining S^{2-} and displaced away from the vacancy. In that case, the twelve Zn second neighbors will no longer be at uniform distances; the Cu–Zn peak splits into three: one at a shorter pair distance, one with the pair distance nearly unchanged, and the third at a longer distance, with the number of Zn neighbors for these peaks in the ratio 3 : 6 : 3. Using the ZnS structure and assuming little distortion of the host lattice, the contraction of the Cu–S bond for the first peak can be directly related to a Cu off-center displacement, d, and hence the distances for the resulting Cu–Zn peaks. The observed shortening of the Cu–S bond by ∼ 0.08 Å corresponds to d = 0.24 Å, and the Cu–Zn peaks will split by roughly ± 0.2 Å. Such a large splitting of the Cu–Zn peaks will dramatically reduce the amplitude of the Cu–Zn peak (the real parts of the FFT are then out of phase) and can easily explain the very small amplitude observed between 3 and 4 Å in the r-space plots.

If instead most of the Cu are in a surface layer of the ZnS NC (to account for the change in PL), then there could also be a reduced number of first neighbor S and second neighbor Zn atoms. We considered this in some detail by simulating the EXAFS assuming there are only three S atom first neighbors (instead of four) and either four or six Zn second neighbors (instead of twelve); we also included a significant broadening of the distribution functions with $\sigma^2 = 0.006$ Å^2 (*i.e.* corresponding to a bond length variation of order 0.08 Å). These simulations are shown in Fig. 3e. Even with such a reduced number of neighbors and a significant broadening, the simulated Cu–Zn second neighbor peak in Fig. 3e is far larger than the Cu K-edge data at 10 K (Fig. 3 a-c). To systematically reduce the Cu–Zn peak to the tiny amplitude observed for every sample would require an additional large broadening $\sigma^2 \sim 0.04$ Å^2.

To test the off-center displaced model (shown in Fig. 6), we carried out a highly constrained fit over the r-range 1.2–3.8 Å, using a sum of the experimental Cu–S function and three Cu–Zn FEFF peaks initially calculated for the Zn–Zn distance (3.8 Å). The Cu–Zn distances in the fit were determined from the contraction of the Cu–S bondlength; if δr_1 is the change in the

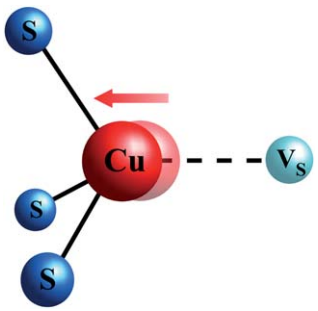

Fig. 6 The local environment about CuS in ZnS showing the Cu (red) displaced away from a S vacancy (light blue) and towards the three remaining S neighbors (blue).

Cu–S bond length, then the changes of the Cu–Zn distances are $2.78\delta r_1$, $-0.114\delta r_1$, and $-2.875\delta r_1$. The Cu–S amplitude was held at the value obtained in the short fits (1.4–2.2 Å) discussed above and the number of neighbors for the three Cu–Zn peaks in the ratio 3 : 6 : 3. Only five parameters were varied: the Cu–S bond length and σ for each peak. An example of such a fit is given in Fig. 7, and the resulting distances are tabulated in Table 2; the variation in the Cu–S bond length between samples is very small, ~ 0.01 Å. Note that in such fits, it is the oscillating real and imaginary parts of the FFT that are fit, not the amplitude envelope. Fig. 7 illustrates how well the phase for the real part of the FFT is modeled over most of the r-space fit range. Although better fits can be obtained by letting the three Cu–Zn distances vary independently, the amplitude of the data is very small and the fractional variation from trace to trace in the 3–4 Å range does not support a more extensive fit.

We noted that if one assumes that the shortened Cu–S distances arise from a [111] displacement of Cu away from the vacancy and towards the three S^{2-}, then the Cu–Zn peak would have a large splitting. A fit based on this model describes the data very well and suggests that the Cu is in a distorted site with Cu^{+}_{Zn} displaced roughly 0.24 Å away from a neighboring S vacancy. Such a distorted Cu site would have C_{3v} symmetry—the symmetry observed in early work by Urabe *et al.*[27] This reduced

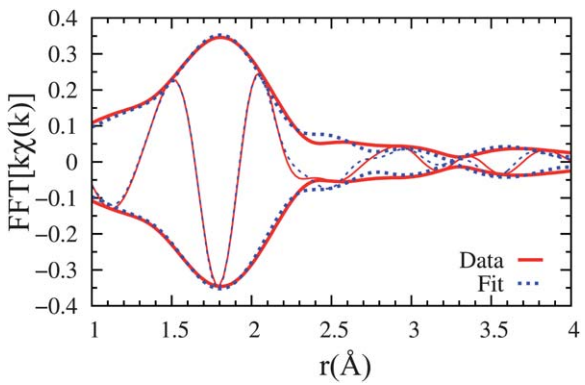

Fig. 7 A fit of the data for sample A2 from 1.2–3.8 Å to a sum of the experimental Cu–S function and three Cu–Zn FEFF functions; the distances for the Cu–Zn functions are calculated from the Cu–S bond contraction as discussed in the text and tabulated in Table 2. Note that only five parameters are varied: δr_1 for the Cu–S peak and σ_i for each peak.

Table 2 Fit results; distances in Å for Cu–S (δr_1 and r_1) and the three Cu–Zn peaks (r_i; i = 2–4) for the off-center Cu model. These are average fits; the relative errors for r_1 are less than 0.01 Å. The third column is the excess broadening (in $Å^2$) of the Cu–S peak relative to the experimental standard

Sample(% Cu)	δr_1	r_1	$(\Delta\sigma)^2$	r_2	r_3	r_4
A1 (0.02)	−0.076	2.267	0.0026	3.615	3.835	4.044
A2 (0.02)	−0.086	2.257	0.0025	3.587	3.837	4.073
A3 (0.02)	−0.085	2.258	0.0025	3.591	3.837	4.069
B1 (0.04)	−0.073	2.272	0.0023	3.623	3.835	4.036
B2 (0.04)	−0.086	2.257	0.0024	3.587	3.837	4.073

symmetry will further split the Cu 3d states; the t_2 states will split into e′ and a_1. Thus, there are three energy levels for Cu on which excited holes may be found: a_1, e′, and e. This might explain the fact that there are three main EL emission lines that decrease in intensity in exactly the same way, as an AC EL device degrades.[13]

It is not clear whether the low concentration S vacancies we find adjacent to Cu^{+}_{Zn} have the same properties as isolated V_S, particularly whether the donor level for V_S in the Cu^{+}_{Zn} -V_S complex is responsible for the trap states 0.6–0.8 eV below the conduction band. Differentiating between these two distinct types of V_S is difficult.

In addition, we note that the excess broadening of the Cu–S peak in fits using the experimental standard (see Table 2) is small, only 0.0023–0.0026 $Å^2$ relative to the experimental standard. Thus although the number of S neighbors is reduced, the disorder of the remaining Cu–S bonds is low.

Finally, we address the possibility of any interstitial Cu, starting with site I_1. In this case, Cu_i provides the charge compensation for a nearby Cu^{+}_{Zn} defect so no S vacancies should be present and a large off-center displacement of Cu_i is not expected for this small fraction of Cu. For each of the samples we carried out another fit, adding a fourth Cu–Zn peak near 2.7 Å, to represent the interstitial Cu–Zn distance in cubic ZnS. Three additional parameters are required for this peak: an amplitude, shift in r (δr_5), and σ_5. In this fit, we started with 0.5 Zn neighbors (*i.e.* ~ 8% Cu_i sites) and constrained the shift of the Cu–Zn distance to ± 0.04 Å about the nominal distance. In all such fits, the amplitude for the interstitial peak goes to zero; there is no significant peak close to 2.7 Å. When we allowed the distance to vary up to ±0.3 Å about the nominal distance, a range of slightly improved fits occur both for significantly longer and shorter distances for r_5. The results varied widely (different amplitudes and σ's); the negative shifts were typically −0.2 Å while positive shifts ranged from 0.2–0.3 Å. Since we are fitting to both the real (R) and imaginary (I) parts of the FFT instead of just the amplitude, the inability to get a fit when we constrain the Cu–Zn distances to ± 0.04 Å indicates that the shape of R and I for the data FFT is quite different than that for the theoretical Cu–Zn function.

The improvement in these fits for large δr_5 was small, considering that three additional parameters are needed to describe the interstitial peak. To quantify the discussion, we used the Hamilton F-test[40] to determine whether adding the extra peak was significant, and applied it to fits for each scan of every sample (25 fits total). Overall, this test indicated that the interstitial peak was not significant, with confidence levels for most

fits being below 67% and well below the necessary 95% confidence level. Fits for a few scans gave confidence levels near 90%, but this is to be statistically expected with 25 fits and the large variation in parameters (amplitudes and σ_5) between fits suggest that the results are dominated by noise.

For the other possible interstitial site, I_2, the closest neighbors are Zn/Cu atoms at approximately 2.34 Å. This interstitial void is large enough to accommodate the large S^{2-} ion, whereas the Cu^{+1} ion is much smaller; however the interaction between Cu_i and the neighboring Zn^{2+} is repulsive. It is thus not clear if the neighboring Zn atoms are displaced. We start assuming the ZnS host lattice is not significantly distorted and generated a Cu–Zn FEFF standard for this pair. Then we fit the first peak in the Cu K-edge data (see Fig. 3) to the sum of the Cu–S experimental peak and the interstitial Cu–Zn peak, starting with various fractions of interstitial site occupations. If we restrict the interstitial Cu–Zn distance to not vary by more than ±0.05 Å, the amplitude of this peak goes to zero and the peak broadens such that the Cu–Zn EXAFS peak has negligible amplitude. Next we let the Cu–Zn distance vary up to ± 0.2 Å. For a large contraction of −0.2 Å, the phase of the real part of the Cu–Zn peak is 180 degrees out of phase with the Cu–S peak and the amplitude is low, corresponding to ~ 2% of the sites. Another fit with a low amplitude is obtained if the distance expands by 0.15 Å to 2.5 Å. We consider these large distortions to be unreasonable for the ZnS lattice. Thus within our uncertainty, the fraction of Cu interstitial sites is very small, no more than 2% and possibly much smaller.

7 Conclusions

We have investigated, for the first time, the local environment about dilute Cu (0.02% and 0.04% Cu) in a number of ZnS:Cu,Cl nanocrystals. From the XANES, we verify that the Cu is in a 1+ oxidation state and using the EXAFS technique, we find that for all samples, the number of S neighbors is significantly below 4 (~3.2), indicating that most Cu atoms have a nearest neighbor S vacancy. In addition, the second neighbor Cu–Zn peak is surprisingly weak, which requires a huge distortion of the Cu–Zn pair distribution function; the amplitude is much smaller than expected for an atom in the surface layer. Furthermore, the Cu–S distance is significantly shorter (~0.07–0.08 Å) than the Zn–S distance in the host.

We noted that if one assumes that the shortened Cu–S distances arise from a [111] displacement of Cu away from the vacancy and towards the three S^{2-}, then the Cu–Zn peak would have a large splitting. A fit using this model, with the shift of the Cu–Zn distances determined from the Cu–S bond contraction, describes the data well. Thus, the EXAFS data suggest that the Cu is in a distorted site with Cu^{+}_{Zn} displaced roughly 0.24 Å away from a neighboring S vacancy, resulting in the Cu site having $\mathbf{C}_{3v}$ symmetry which would further split the Cu 3d states, leaving three energy levels on which excited holes may be found.

Finally, we considered the possibility of some interstitial Cu_i sites which would charge compensate Cu^{+}_{Zn} defects but should have no nearby vacancies. Site I_1, has a distinctive signature—a Cu–Zn peak at a rather short distance of 2.7 Å. Adding a peak at this distance did not significantly improve the fits, and if the distance was constrained to be close to the expected distance, the amplitude of the peak went to zero. The second site I_2 has four nearest neighbor Zn/Cu atoms at the normal Cu–S distance (2.34 Å). Including a very short Cu–Zn/Cu peak (near 2.34 Å) in the fit did not improve the fit significantly and if the distance was constrained within ± 0.05 Å, the amplitude went to zero. Thus, we conclude that if there are Cu_i sites, the fraction of Cu_i sites must be very small, < 2% of the total Cu sites. These results provide a better fundamental understanding of the local structure of the Cu dopant in ZnS nanocrystals, which is significant for understanding the PL emission centers and for applications including electroluminescence.

Acknowledgements

This project was funded by the Department of Energy (DE-FG02-07ER46388). The EXAFS experiments were performed at SSRL, and Office of Science User Facility operated for the DOE by Stanford University.

References

1 S. Shionoya, *Phosphor Handbook*, CRC Press, New York, 1999, (ch. 3), pp. 231–258.
2 S. Tanaka, H. Kobayashi and H. Sasakura, *Phosphor Handbook*, CRC Press, New York, 1999, (ch. 9), pp. 601–612.
3 G. Destriau, *J. Chem. Phys.*, 1936, **33**, 620.
4 A. A. Bol, J. Ferwerda, J. A. Bergwerff and A. Meijerink, *J. Lumin.*, 2002, **99**, 325–334.
5 Y.-T. Nien and I.-G. Chen, *Appl. Phys. Lett.*, 2006, **89**, 261906.
6 M. Warkentin, F. Bridges, S. A. Carter and M. Anderson, *Phys. Rev. B: Condens. Matter Mater. Phys.*, 2007, **75**, 075301/1–9.
7 W. Wang, F. Huang, Y. Xia and A. Wang, *J. Lumin.*, 2008, **128**, 610.
8 S. S. Nath, D. Chakdar, G. Gope, J. Kakati, B. Kalita, A. Talukdar and D. K. Avasthi, *J. Appl. Phys.*, 2009, **105**, 94305.
9 C. Corrado, Y. Jiang, F. Oba, M. Kozina, F. Bridges and J. Z. Zhang, *J. Phys. Chem. A*, 2009, **113**, 3830.
10 J. Manam, V. Chatterjee, S. Das, A. Choubey and S. K. Sharma, *J. Lumin.*, 2010, **130**, 292–297.
11 D. Jiang, L. Cao, W. Liu, G. Su, H. Qu, Y. Sun and B. Dong, *Nanoscale Res. Lett.*, 2009, 4, pp. 78–83.
12 R. S. Gupta, J. Kaur, N. S. Suryanarayana and V. Dubey, *Int. J. of Nanotech. and Applications*, 2010, **4**, 185–188.
13 J. Stanley, Y. Jiang, F. Bridges, S. A. Carter and L. Ruhlen, *J. Phys.: Condens. Matter*, 2010, **22**, 055301(15).
14 A. G. Fischer, *J. Electrochem. Soc.*, 1963, **110**, 733–48.
15 J. S. Prener and F. E. Williams, *J. Chem. Phys.*, 1956, **25**, 361.
16 A. A. Khosravi, M. Kundu, L. Jatwa, S. K. Deshpande, U. A. Bhagwat, M. Sastry and S. K. Kulkarni, *Appl. Phys. Lett.*, 1995, **67**, 2702–2704.
17 M. Wang, L. Sun, X. Fu, C. Liao and C. Yan, *Solid State Commun.*, 2000, **115**, 493–496.
18 K. Sooklal, B. S. Cullum, S. M. Angel and C. J. Murphy, *J. Phys. Chem.*, 1996, **100**, 4551–4555.
19 W. Peng, G. Cong, S. Qu and Z. Wang, *Opt. Mater.*, 2006, **29**, 313–317.
20 K. Manzoor, S. R. Vadera, N. Kumar and T. R. N. Kutty, *Mater. Chem. Phys.*, 2003, **82**, 718–725.
21 S. Lee, D. Song, D. Kim, J. Lee, S. Kim, I. Y. Park and Y. D. Choi, *Mater. Lett.*, 2004, **58**, 342–346.
22 E. F. Apple and J. S. Prener, *J. Phys. Chem. Solids*, 1960, **13**, 81–87.
23 A. Suzuki and S. Shionoya, *J. Phys. Soc. Jpn.*, 1971, **31**, 1455–1461.
24 R. Bowers and N. T. Melamed, *Phys. Rev.*, 1955, **99**, 1781–87.
25 W. C. Holton, M. de Wit, R. K. Watts, T. L. Estle and J. Schneider, *J. Phys. Chem. Solids*, 1969, **30**, 963–977.
26 S. Shionoya, K. Urabe, K. Era and H. Fujiwara, *J. Phys. Chem. Solids*, 1966, **27**, 865–69.
27 K. Urabe, S. Shionoya and A. Suzuki, *J. Phys. Soc. Jpn.*, 1968, **25**, 1611–1617.
28 S. Shionoya, T. Koda, K. Era and H. Fujiwara, *J. Phys. Soc. Jpn.*, 1964, **19**, 1157–67.
29 H. Blicks, N. Riehl and R. Sizmann, *Z. Phys.*, 1961, **163**, 594–603.
30 W. A. Thornton, *Phys. Rev.*, 1956, **102**, 38–46.

31 See http://lise.lbl.gov/RSXAP/.
32 H. J. Sánchez, M. C. Valentinuzzi and C. Pérez, *J. Phys. B: At., Mol. Opt. Phys.*, 2006, **39**, 4317–4327.
33 S. Medling and F. Bridges, *J. Synchrotron Radiat.*, 2011, **18**, 679–680.
34 B. K. Teo, *EXAFS: Basic Principles and Data Analysis*, Springer-Verlag, New York, 1986.
35 A. L. Ankudinov, B. Ravel, J. J. Rehr and S. D. Conradson, *Phys. Rev. B: Condens. Matter Mater. Phys.*, 1998, **58**, 7565.
36 J. J. Rehr, private communication.
37 Z. Kvitky, F. Bridges and G. van Dorssen, *Phys. Rev. B: Condens. Matter*, 2001, **64**, 214108/1–11.
38 G. G. Li, F. Bridges and C. H. Booth, *Phys. Rev. B: Condens. Matter*, 1995, **52**, 6332–48.
39 F. Bridges, L. Downward, J. J. Neumeier and T. A. Tyson, *Phys. Rev. B: Condens. Matter Mater. Phys.*, 2010, **81**, 184401.
40 L. Downward, C. H. Booth, W. W. Lukens and F. Bridges, *X-ray Absorption Fine Structure - XAFS13*: 13th International Conference, New York, 2006.